RSC Advances

ROYAL SOCIETY OF CHEMISTRY

www.rsc.org/advances

Monodispersed hierarchical γ-AlOOH/$Fe(OH)_3$ micro/nanoflowers for efficient removal of heavy metal ions from water

Yongxing Zhang[1], Xiangbo Zhou[1], Zhongliang Liu[1], Bing Li[1], Qiangchun Liu[1], and Xuanhua Li[2*]

[1]Collaborative Innovation Center of Advanced Functional Composites, Huaibei Normal University, Huaibei 23500, P. R. China

[2]Center of Nano Energy Materials, State Key Laboratory of Solidification Processing, School of Materials Science and Engineering, Northwestern Polytechnical University Xi'an 710072, P. R. China

E-mail: lixh32@nwpu.edu.cn

Abstract

Many nanomaterials have been reported for removal of toxic inorganic metal ions. Some conventional micro- or nano-structured adsorbents are subject to serious aggregation. Here, the well-dispersed, $Fe(OH)_3$ colloid nanoparticles have been effectively deposited onto the surfaces of the hierarchical γ-AlOOH nanostructures to form the γ-AlOOH/$Fe(OH)_3$ with hierarchical structures via an electrostatic attraction without forming large aggregates. The monodispersed γ-AlOOH/$Fe(OH)_3$ with hierarchical structures have high specific surface areas and large pore volumes, which are used as adsorbents to remove anion species of As(V) and Cr(VI) from aqueous solution. The maximum capacities of the monodispersed γ-AlOOH/$Fe(OH)_3$ with hierarchical structures for As(V) and Cr(VI) in this study are determined at 43.8 mg g^{-1} and 13.1 mg g^{-1},

respectively, which are higher than those of the other metal oxide nanostructures reported to date. In addition, the adsorption rates of As(V) and Cr(VI) onto the monodispersed γ-AlOOH/$Fe(OH)_3$ with hierarchical structures are rather fast. The γ-AlOOH/$Fe(OH)_3$ hierarchical micro/nanoflower structures show high adsorption capacity for removing anion species of As(V) and Cr(VI), demonstrating a promising potential in environmental remediation.

Key words: hierarchical nanostructures, γ-AlOOH/$Fe(OH)_3$ nanomaterials, heavy metal ions, Adsorbents.

1. Introduction

Removal of heavy metal ions from water has received popular attention due to its significance in the protection of human health. In recent years, among various purification methods, an adsorption approach has been of great interest because of its low cost, easy construction and operation.[1-7] Recently, nanostructured adsorbents have been considered promising candidates because of their large surface area, high surface activity, and ease of modification with more specifically functional groups.[8-12] However, the small size of nanostructured adsorbents increases the likelihood of substantial aggregation during the adsorption process. Numerous adsorption sites of the materials are covered, making interaction with pollutants like heavy metal ions or organic molecules in water difficult, thereby greatly reducing the adsorption efficiency. In these conditions, the potential benefits of nanostructures are hardly utilized; thus, there remains the challenge of making these advantages of nanostructures effective for adsorbing pollutants.[13-20]

Metal oxide micro/nanomaterials with well-defined structures, as one of the most promising

adsorbents, have been widely studied due to their large surface areas, high available surface adsorption site density, special functionality and well-defined morphology.[11, 21-24] The natures of the metal oxide micro/nanomaterials with well-defined structures remarkably enhance their physical chemical adsorption. Among these metal oxide micro/nanomaterials with well-defined structures, Boehmite (γ-AlOOH) has been recognized as an efficient inorganic adsorbent due to its excellent physical-chemical properties and low toxicity.[25-33] Controlling the size and shape of γ-AlOOH nanostructures plays a key role in improving the properties of the final alumina materials. [33, 34] Up to now, various nanostructures of γ-AlOOH, such as hierarchical structures of γ-AlOOH nanoflakes, [35] leaf-like micro/nanoarchitectures, [36] broccoli-like structures,[37] urchin-like hollow microspheres, [38-41] Self-curled coral-like nanoplates,[42] fiber-like morphologies[34] and other hierarchical structures[33, 43-45] have been synthesized by different methods. However, it still remains a challenge to develop a facile and environmentally friendly method for obtaining monodispersed, uniform, and flower-like hierarchical γ-AlOOH with ultrathin lamellar structures.

The $Fe(OH)_3$ colloid nanoparticles can be used as adsorbents for the removal of anion pollutant from water due to their large specific surface area and high available surface adsorption site density.[46] However, on the basis of practicality, the particles with nanometer size create some difficulties in the separation and recycling of the adsorbents from suspension after application in water and wastewater treatment, which hinders their industrial applications that are too fine to be removed by gravitational settling due to the strong Brownian motion. In addition, nanoparticles aggregation during adsorption processes limits their adsorption activity. Therefore, the search for $Fe(OH)_3$ colloid particles with high adsorption capacity, which can be easily separated from liquid phase by natural settlement in a short time is still a big challenge.

Herein, we synthesize monodispersed, uniform, and flower-like γ-AlOOH/$Fe(OH)_3$ composites. These monodispersed hierarchical γ-AlOOH/$Fe(OH)_3$ micro/nanoflowers for the removal of heavy metal ions from water have the following features: (a) they are of low cost and nontoxic, which can be achieved by using low cost and nontoxic raw materials, and low cost synthesis methods. (b) their nanostructures provide the high surface area as well as the high removal capacity for heavy metal ions. (c) the monodispersed hierarchical alumina materials (γ-AlOOH samples), used as adsorbent supports, could prevent the agglomerate problem caused by high surface energy and Van der Waals force between the $Fe(OH)_3$ colloid nanoparticles.

2. Experimental section

All reagents were of an analytical grade and are commercially available from Sinopharm Chemical Reagent Co., Ltd (China) and were used without further purification.

2.1. Preparation of monodispersed hierarchical γ-AlOOH micro/nanoflowers

In a typical experiment, 1.02 g of sodium aluminate ($NaAlO_2$), 8.67g of urea (H_2NCONH_2) and 0.20 g polyacrylic acid sodium salt (MW $\geqslant 3.0 \times 10^7$) was dissolved in 30 mL of deionized water under stirring. After being stirred for 30 min, the solution was transferred into a 40 mL Teflon-lined stainless steel autoclave, sealed and maintained at 140 ^oC for 10 h. After the reaction system was naturally cooled to room temperature, the white precipitates was separated from solution and thoroughly washed several times with deionized water and absolutely ethanol, and then dried in a vacuum oven at 50 ^oC for 12 h.

2.2. Preparation of the monodispersed hierarchical γ-AlOOH/Fe(OH)$_3$ micro/nanoflowers

The monodispersed hierarchical γ-AlOOH/Fe(OH)$_3$ micro/nanoflowers were prepared by boiling forcing-hydrolysis method. In a typical synthesis, the monodispersed hierarchical γ-AlOOH micro/nanoflowers (50 mg) were well dispersed in 25 ml deionized water. Subsequently, the above solution was heated to boiling. Then, 5 ml of the saturated ferric chloride solution was added dropwise to the boiling solution. Continue to boil the solution until it became reddish brown, turn off the heat. After the reaction system was naturally cooled to room temperature, the precipitates was separated from solution and thoroughly washed several times with deionized water and absolutely ethanol, and then dried in a vacuum oven at 50 ^{o}C for 6h.

2.3. Adsorption experiments

For the equilibrium adsorption isotherm study, the adsorption experiments were carried out in a serial of 15 mL glass vials, equipped with aluminum foil-lined teflon screw caps. Adsorbents and As(V) or Cr(VI) aqueous solution were added to the glass vial (Na_3AsO_4 •$12H_2O$ and $K_2Cr_2O_7$ were used as the sources of As(V) and Cr(VI), respectively). Samples were shaken for 24 h in order to achieve adsorption equilibrium. After the adsorption, adsorbents were separated using centrifugation. The adsorption capacity of the adsorbents was measured by the difference between the initial and remaining concentrations of As(V) or Cr(VI). The equilibrium adsorption capacity, q_e (mg g^{-1}), was calculated by:

$$q_e = \frac{V(Co\text{-}Ce)}{W} \qquad (1),$$

where C_o is the initial concentration of As(V) or Cr(VI) (mg L^{-1}); C_e is the equilibrium concentration (mg L^{-1}); V is the volume of the solution used (L); and W is the weight of the

adsorbents (g). The adsorption capacity of the adsorbents at time t, q_t (mg g^{-1}), was also calculated:

$$q_t = \frac{V(C_o - C_t)}{W} \quad (2),$$

where C_t is the concentration of As(V) or Cr(VI) at contact time t (mg L^{-1}).

All the adsorption experiments were carried out at room temperature (298 ± 2 K). All the experimental data were the average of triplicate determinations. The relative errors of the data were about 5%.

2.4. Characterization

X-ray diffraction (XRD) patterns were obtained in the 2ɵ range of 10-70° using a Philips X'Pert Pro X-ray diffractometer with Cu Kα radiation (1.5418Å). Field emission scanning electron microscope (FESEM) images were taken on a FESEM (Quanta 200 FEG) operated at an accelerating voltage of 10.0kV. Transmission electron microscope (TEM) images were obtained on a JEOL JEM-2010 high resolution transmission electron microscope, equipped with X-ray energy dispersive spectroscopy (EDS) capabilities, working at an acceleration voltage of 200 kV. The specific surface areas of the samples were measured with Micromeritics ASAP 2020 M^+C Brunauer-Emmet-Teller (BET) equipment by using nitrogen adsorption and desorption. The As(V) and Cr(VI) concentrations were determined in the liquid phase using inductively coupled plasma atomic emission spectrometry (ICP-AES, Jarrell-Ash model ICAP 9000).

3. Results and discussion

The goal for preparation of γ-AlOOH/$Fe(OH)_3$ is to efficient removal of the anion species of As(V) and Cr(VI) from water. A series of experimental results are carried out for demonstrating this issue,

including the structural and morphological characteristics, BET evaluation and As(V) and Cr(VI) removal from water.

3.1 Preparation of γ-AlOOH and γ-AlOOH/$Fe(OH)_3$ micro/nanoflowers

The synthetic procedure for the monodispersed nanoflowers γ-AlOOH/$Fe(OH)_3$ is illustrated in Scheme 1. Firstly, γ-AlOOH micro/nanoflowers with ultrathin lamellar structures are prepared, which is found to possess a weak adsorption capacity for heavy metal anion As(V) and Cr(VI) (see Fig. 5). To solve the problem, some further modifications have been conducted. Namely, γ-AlOOH micro/nanoflowers are used as adsorbent supports, and $Fe(OH)_3$ colloid nanoparticles have been effectively deposited onto the surfaces of the hierarchical γ-AlOOH nanostructures to form the γ-AlOOH/$Fe(OH)_3$ with hierarchical structures via an electrostatic attraction without forming large aggregates. The γ-AlOOH/$Fe(OH)_3$ hierarchical structures show high adsorption capacity for removing anion species of As(V) and Cr(VI).

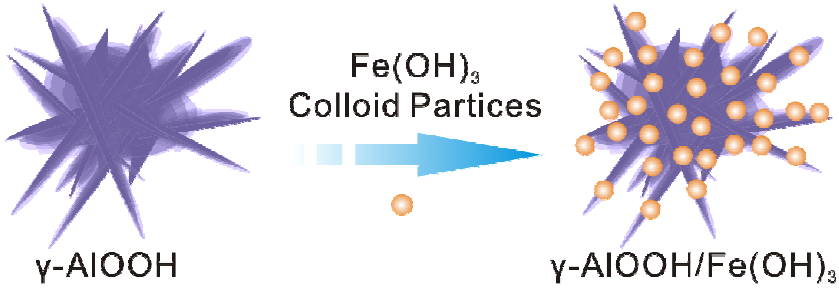

Scheme 1. Boiling forcing-hydrolysis method for the formation of the γ-AlOOH/$Fe(OH)_3$ micro/nanoflowers.

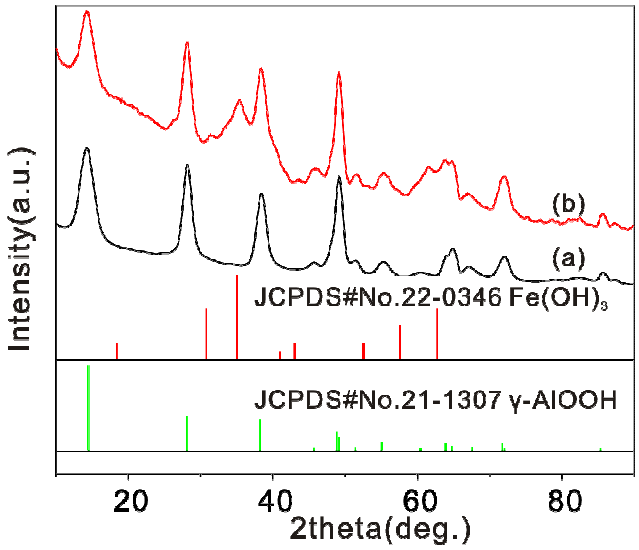

Fig. 1. XRD patterns of the γ-AlOOH and γ-AlOOH/$Fe(OH)_3$ micro/nanoflowers.

γ-AlOOH micro/nanoflowers are firstly prepared and measured. The formation of crystalline γ-AlOOH in the hydrothermal process is confirmed by XRD pattern in the curve (a) of Fig. 1 (JCPDS Card 21-1307). Fig. 2(a) and (b) show the scanning electron microscope (SEM) image of the as-prepared γ-AlOOH nanomaterials, from which it can be clearly seen that the sample is composed of many nearly monodispersed hierarchical γ-AlOOH micro/nanoflowers with a diameter of approximately 700 nm. The detailed morphology of the micro/nanoflowers is shown in Fig. 2(c), which reveals that the structure is composed of many nanosheets with a thickness of 3-8 nm. The flower-like product is further revealed by the transmission electron microscopy (TEM) images in Fig. 2(d) and (e), from which it is apparent that the structure is assembled by some nanosheets. Fig. 2(f) reveals the high-resolution TEM images of the nanosheet, which clearly indicate that the nanosheet is a curving lamella with a thickness of ca. 3.0 nm. It is noted to say that the as-prepared nanoflowers are monodispersed and can be well dispersed in the solution without large aggregation (Fig. 2).

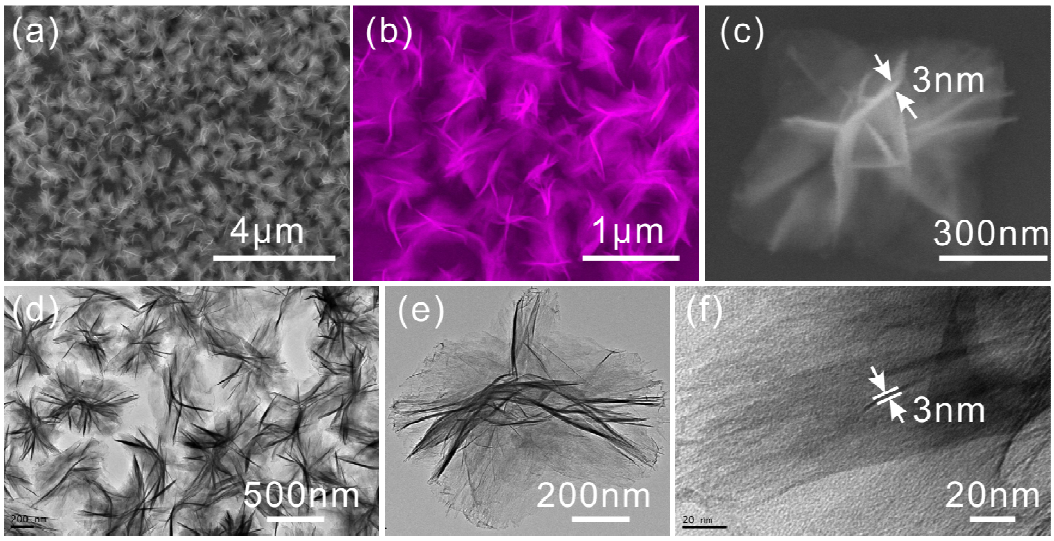

Fig. 2. (a)-(c) SEM and (d)-(f) TEM images of the γ-AlOOH micro/nanoflowers.

The $Fe(OH)_3$ colloid nanoparticles can be effectively self-assembled onto the surfaces of the hierarchical γ-AlOOH nanosheets to form the γ-AlOOH/$Fe(OH)_3$ micro/nanoflowers via an electrostatic attraction without forming large aggregates (Scheme 1). In general, the surface properties of the γ-AlOOH are based on the presence of the functional groups. In near neutral aqueous environments, lamellar γ-AlOOH has a large number of surface hydroxyl groups. The groups cause the surface to have negatively charged due to the terminal OH sites. Thus, the positive charged $Fe(OH)_3$ colloid nanoparticles can be well effectively dispersed on the negatively charged surface of γ-AlOOH nanosheets via electrostatic attraction[47-49].

The XRD pattern of the γ-AlOOH/$Fe(OH)_3$ micro/nanoflowers (the curve (b) in Fig. 1) show that, compared with the curve (a) in Fig. 1, additional peaks appear, which can be attributed to the phase of $Fe(OH)_3$ colloid nanoparticles (JCPDS Card 22-0346). This suggests that this sample contains $Fe(OH)_3$ phases. However, because of the low content of $Fe(OH)_3$, the intensity of the XRD pattern of $Fe(OH)_3$ is weak.

Fig. 3 (a) and (b) show the SEM images of the γ-AlOOH/$Fe(OH)_3$ micro/nanoflowers. From

the figures, it is clear that the obtained products still maintain the uniform-sized, flower-like and hierarchical structures. TEM images (Fig. 3(c) and (e)) are also used to examine the structures of the γ-AlOOH/$Fe(OH)_3$ micro/nanoflowers. Compared with Fig. 2(e) and (f), Fig.3 (c) and (e) clearly indicate that the $Fe(OH)_3$ colloid nanoparticles are successfully self-assembled on the surface of the hierarchical γ-AlOOH nanosheets via electrostatic attraction. These small size nanoparticles are well dispersed on the surface of the hierarchical γ-AlOOH nanosheets, which are more beneficial to further increasing the BET surface area of the γ-AlOOH/$Fe(OH)_3$ micro/nanoflowers. The energy dispersive spectroscopic (EDS) analysis (Fig. 3(d)) of the sample reveals the existence of O, Al and Fe elements. The Cu signal originates from the copper TEM grid. In order to further confirm the presence of the $Fe(OH)_3$ colloid nanoparticles on the surface of the γ-AlOOH/$Fe(OH)_3$ micro/nanoflowers, samples are analyzed by electron mapping image analysis (Fig. 3(f)-(h)). The images are acquired by visualizing the inelastically scattered electrons in the energy loss windows for elemental O, Al, and Fe. The different color areas shown in parts (f)-(h) of Fig. 3 indicate O-, Al-, and Fe-enriched areas of the sample, respectively. The images also show that the $Fe(OH)_3$ colloid nanoparticles are well dispersed on the surface of the γ-AlOOH micro/nanoflowers. In addition, the exact loading of $Fe(OH)_3$ nanoparticles (mol %) is 18.27, which has been characterized by the inductively coupled plasma mass spectrometry (Agilent7500CS).

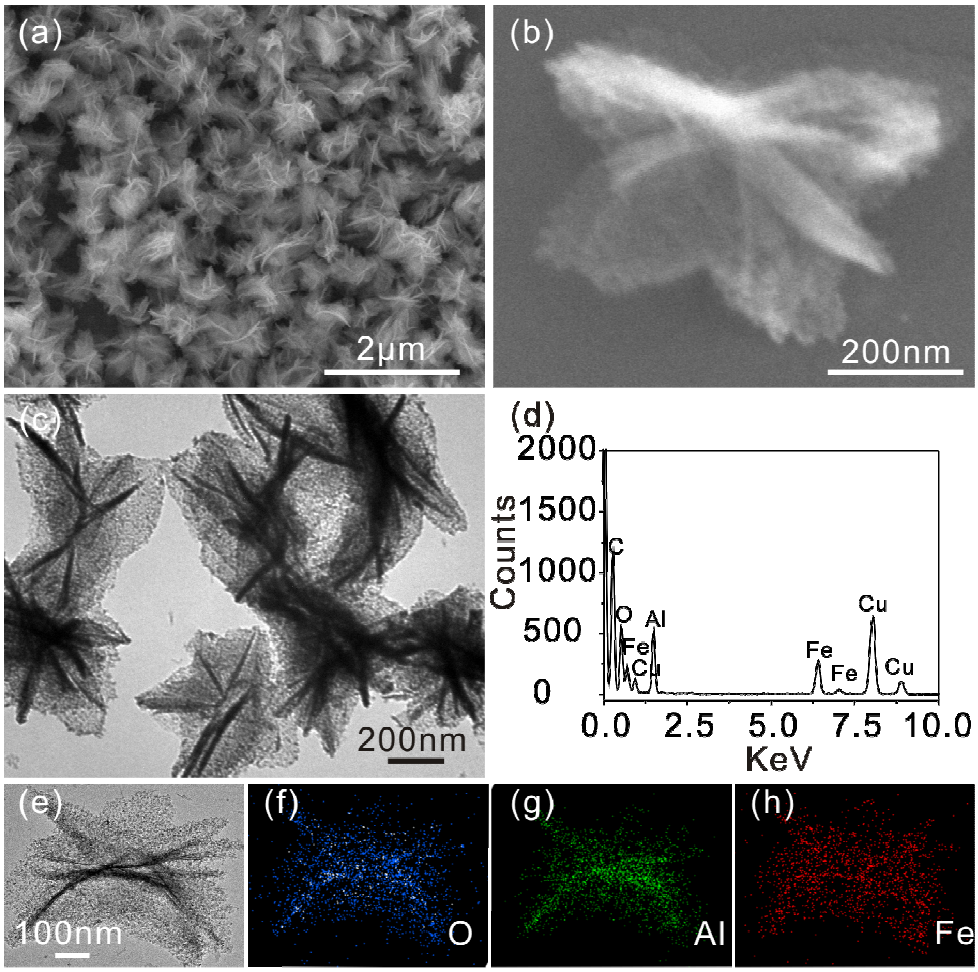

Fig. 3. (a) and (b) SEM, (c) and (e) TEM images and (d) EDS spectrum of γ-AlOOH/$Fe(OH)_3$ micro/nanoflowers. Electron energy loss (f) "O", (g) "Al" and (h) "Fe" element mapping images of γ-Al_2O_3/$Fe(OH)_3$ micro/nanoflowers. In Fig. 5(f), (g) and (h), blue, green and red areas indicate "O", "Al" and "Fe" enriched parts of γ-AlOOH/$Fe(OH)_3$ micro/nanoflowers, respectively.

To characterize the specific surface areas and porosities of the as-prepared samples, N_2 adsorption analysis is carried out. Fig. 4 present the nitrogen adsorption-desorption isotherms and BJH pore size distribution curves of the γ-AlOOH and γ-AlOOH/$Fe(OH)_3$ respectively. For the γ-AlOOH micro/nanoflowers, the BET surface area and the pore volume have been estimated to be 145.523 m^2 g^{-1} and 0.396 cm^3 g^{-1}, respectively. The pore size distribution curve exhibits a broad

peak in the range of 10-100 nm with a maximum at 90 nm. The result indicates that there are some mesopores/macropores in the sample. The mesopores reflect porosity between the nanosheets which formed the γ-AlOOH micro/nanoflowers, while larger mesopores/macropores can be related to the pores formed between the γ-AlOOH micro/nanoflowers. These mesoporous/macroporous structures can be directly observed from the SEM and TEM images of the samples shown in Figure 2. Fig. 4 (b) and (d) present the nitrogen adsorption-desorption isotherms and BJH pore size distribution curves of the γ-AlOOH/$Fe(OH)_3$ micro/nanoflowers. The shape of the hysteresis loops is very similar to that of the γ-AlOOH micro/nanoflowers. These results indicate that the pore structures are preserved during deposition of $Fe(OH)_3$ colloid nanoparticles. For the γ-AlOOH/$Fe(OH)_3$ micro/nanoflowers, the BET surface area and the pore volume have been estimated to be 171.249 $m^2\ g^{-1}$ and 0.400 $cm^3\ g^{-1}$, respectively. The pore size distribution curve exhibits a broad peak in the range of 10-100 nm with a maximum at 15 nm. From these data, the BET specific surface area of the γ-AlOOH/$Fe(OH)_3$ is higher than that of the γ-AlOOH. The increase is attributed to the surface roughness caused by the deposition of $Fe(OH)_3$ colloid nanoparticles.

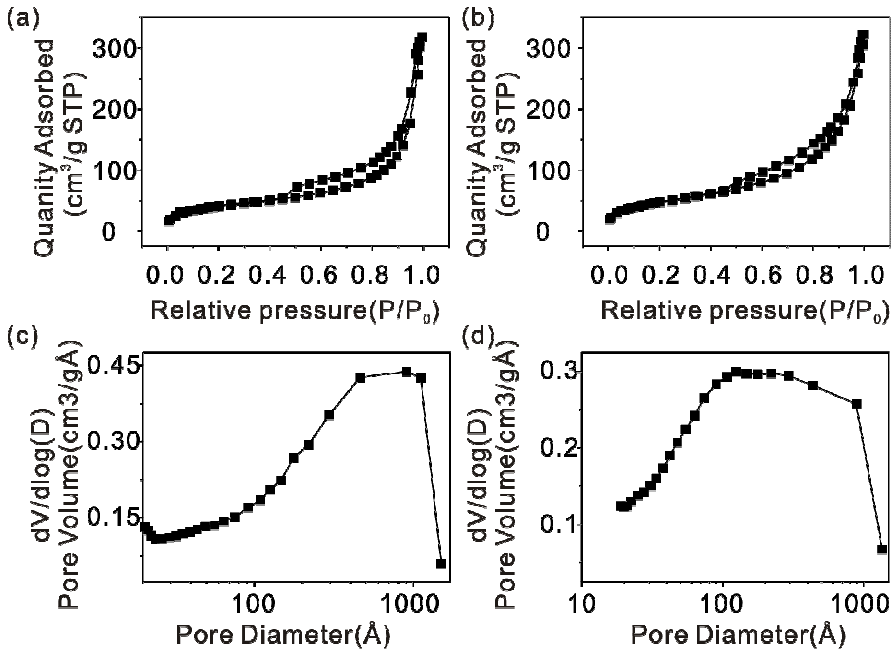

Fig. 4. Nitrogen adsorption/desorption isotherm of (a) γ-AlOOH and (b) γ-AlOOH/$Fe(OH)_3$ micro/nanoflowers; BJH pore size distribution plot of (c) γ-AlOOH and (d) γ-AlOOH/$Fe(OH)_3$ micro/nanoflowers

Monodispersed hierarchical micro/nanostructured materials can avoid aggregation and maintain the high specific surface areas, high value of pore volume and ideal pore size distribution which are important in enhancing the accessibility of adsorbents to reactive sites.[50] As is well known, As(V) and Cr(VI) are considered to highly toxic water pollutants, and their efficient removal from water is of great importance. Herein, we investigate the capacity of these samples to remove As(V) and Cr(VI) ions from aqueous solutions (Fig. 5). As shown in Fig. 5(a), the adsorption capacity of γ-AlOOH/$Fe(OH)_3$ micro/nanoflowers is higher than that of γ-AlOOH micro/nanoflowers for As(V) and Cr(VI). It is found that γ-AlOOH micro/nanoflowers have few adsorption for As(V) and Cr(VI) ions. Two empirical equations, the Langmuir and Freundlich isotherm models, are used to analyze the experimental data. The mathematical expressions of the Langmuir isotherm and the Freundlich isotherms model are. [51-53]

$$\frac{C_e}{q_e} = \frac{1}{q_m K_L} + \frac{C_e}{q_m} \quad (3)$$

$$\ln q_e = \frac{1}{n} \ln C_e + \ln K_F \quad (4)$$

where q_m and K_L are Langmuir constants, representing the maximum adsorption capacity of adsorbents (mg g^{-1}) and the energy of adsorption, respectively. K_F and n are Freundlich constants related to adsorption capacity and adsorption intensity, respectively.

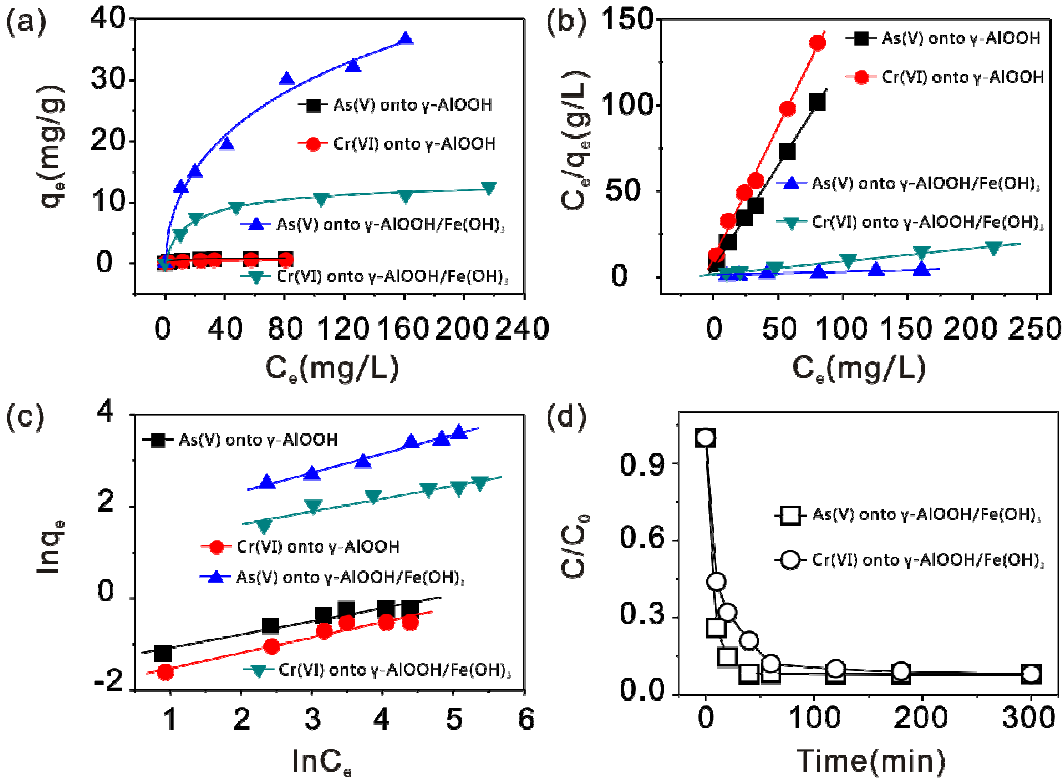

Fig. 5. (a) Adsorption isotherms, (b) Linearized Langmuir isotherms and (c) Linearized Freundlich isotherms of As(V)/Cr(VI) onto γ-AlOOH, and γ-AlOOH/$Fe(OH)_3$ micro/nanoflowers; (d) Adsorption rate of As(V) (initial concentration of 6.2 mg L^{-1})/Cr(VI) (initial concentration of 3.1 mg L^{-1}) onto the as-prepared γ-AlOOH/$Fe(OH)_3$ micro/nanoflowers

For the Langmuir isotherm model, the values of q_m and K_L can be calculated from the slope and intercept of plots of C_e/q_e versus C_e. For the Freundlich isotherm model, the values of n and K_F can be obtained by a plot of lnq_e against lnC_e. The Linearized Langmuir isotherms (Fig. 5(b)) and

Linearized Freundlich isotherms (Fig. 5(c)) of As(V)/Cr(VI) onto γ-AlOOH/$Fe(OH)_3$ micro/nanoflowers are also shown. The parameters of the Langmuir and Freundlich models are calculated and listed in Table 1. The maximum capacities of γ-AlOOH and γ-AlOOH/$Fe(OH)_3$ micro/nanoflowers for As(V)/Cr(VI) are determined at 0.84/0.65 mg g^{-1} and 43.8/13.1 mg g^{-1}, respectively. From the correlation coefficients, it can be seen that the adsorption data for As(V)/Cr(VI) fit the Langmuir isotherm model better than the Freundlich isotherm model. In addition, the maximum adsorption capacities of these samples for As(V) are better than that of Cr(V). Further work is underway to investigate the reason for this point.

Table 1. Equilibrium adsorption isotherm fitting parameters for As(V) and Cr(VI) onto γ-AlOOH and γ-AlOOH/$Fe(OH)_3$ micro/nanoflowers, respectively.

Absorbent samples	As						Cr					
Models	Langmuir			Freundlich			Langmuir			Freundlich		
Parameters	q_{max}	K_L	R^2	K	1/n	R^2	q_{max}	K_L	R^2	K	1/n	R^2
Gamma-AlOOH	0.84	0.21	0.99	0.25	0.28	0.90	0.65	0.14	0.99	0.15	0.33	0.92
Gamma-AlOOH/$Fe(OH)_3$	43.80	0.02	0.98	4.46	0.41	0.97	13.10	0.052	0.99	2.87	0.27	0.92

The results are also significantly higher than that of reported related adsorbents, such as flowerlike α-Fe_2O_3, Commercial α-Fe_2O_3, flowerlike CeO_2, Spindle-like γ-Al_2O_3, annealed hierarchical SiO_2@γ-AlOOH spheres, akaganeite (β-FeOOH) nanorods and hollow magnetic porous Fe_3O_4/α-FeOOH microspheres (Table 2). The high adsorption capacities of these samples are due to the higher specific area, the novel hierarchical nanostructures and different anion uptake

mechanisms. More importantly, most results reported in the literatures are obtained at low pH values for As(V) and Cr(VI), thus those good removal performances may not be realized at normal pH values in practical water purification. While in this study the removal capacity values of the monodispersed hierarchical aluminum/iron oxides micro/nanoflowers are measured under neutral pH values.

Table 2. Comparison of our work with some metal oxides reported for removal of As(V) and Cr(VI) ions.

Adsorbents	qm (mg g-1)		References
	As(V)	*Cr(VI)*	
γ-AlOOH micro/nanoflowers	0.84	0.65	This study
γ-AlOOH/Fe(OH)3 micro/nanoflowers	**43.8**	**13.1**	**This study**
Flowerlike α-Fe2O3	7.6	5.4	[50]
Commercial α-Fe2O3	0.3	0.37	[54]
Flowerlike CeO2	14.4	5.9	[21]
Spindle-like γ-Al2O3	—	6.70	[33]
Annealed hierarchical SiO2@γ-AlOOH spheres	—	4.7	[55]
Akaganeite (β-FeOOH) nanorods	29.0	—	[56]
Hollow magnetic porous Fe3O4/α-FeOOH microspheres	30.2	—	[57]

In addition, we also study the kinetics of adsorption, which is one of the most important characteristics that define the efficiency of adsorption. The kinetics of adsorption describes the solute uptake rate governing the residence time of the adsorption reaction. Because γ-AlOOH micro/nanoflowers have few adsorption for As(V) and Cr(VI) ions, we focus to study the kinetics

of adsorption for γ-AlOOH/$Fe(OH)_3$ micro/nanoflowers. In the kinetic study of As(V)/Cr(VI) adsorption on the as-prepared γ-AlOOH/$Fe(OH)_3$ micro/nanoflowers, the initial As(V) and Cr(VI) concentrations are 6.2 and 3.1 mg L^{-1} , respectively. The experiments are carried out using a 250 mL conical flask containing 100 mL of an As(V)/Cr(VI) solution, and the adsorbent dose is 0.2 g L^{-1} in the kinetics study. These samples are placed on a shaker for stirring. At predetermined time intervals, stirring is interrupted while 5 mL of supernatant solutions are pipetted and centrifuged for the determination of the remaining As(V)/Cr(VI) concentrations. The kinetics of As(V)/Cr(VI) adsorption onto the as-prepared γ-AlOOH/$Fe(OH)_3$ micro/nanoflowers are shown in Fig. 5(d). It is clear that the adsorption rates of As(V) onto the γ-AlOOH/$Fe(OH)_3$ micro/nanoflowers are faster than and Cr(VI) onto the γ-AlOOH/$Fe(OH)_3$ micro/nanoflowers. The adsorption mechanism of As(V) and Cr(VI) ions can be explained as follows: The As(V) and Cr(VI) ions mainly existed in the form of $HAsO_4^{2-}$ and $HCrO_4^-$ in acidic conditions.[18, 58] For γ-AlOOH/$Fe(OH)_3$ micro/nanoflowers, the positive charged $Fe(OH)_3$ colloid nanoparticles being dispersed on the surface of the γ-AlOOH micro/nanoflowers can interact with the negatively charged anionic $HAsO_4^{2-}$ and $HCrO_4^-$ species via electrostatic attraction.

4. Conclusions

In summary, we have used $NaAlO_2$, a nontoxic and inexpensive reagent, to synthesize monodispersed hierarchical γ-AlOOH micro/nanoflowers. γ-AlOOH/$Fe(OH)_3$ micro/nanoflowers could be obtained from the γ-AlOOH precursor without changing their morphologies via boiling forcing-hydrolysis method. This sample has high BET surface areas and large pore volumes. Its novel micro/nanocomposite structure possesses the advantages of both microstructure and

nanostructure. The as-obtained monodispersed hierarchical aluminum/iron oxides micro/nanoflowers are effective sorbents for the removal of As(V) and Cr(VI) in water treatment due to the high available surface adsorption site density, its larger specific surface area and pore volume. And it should be a promising material for environmental application. This study also shows that the efficient adsorbents for highly toxic metal ions removal can be designed by depositing nanoparticles with high adsorption capacity on mesoporous supports with abundance of surface hydroxyls and large surface area.

Acknowledgements

This research was supported by the National Natural Science Foundation of China (51302102 51402120, 11504120, 51571166 and 61505167), the Natural Science Foundation of Anhui Province (1408085QA19), the Natural Science Research Project for Colleges and Universities of Anhui Province (KJ2014A222), the Huaibei Scientific Talent Development Scheme (20140305 and 20140311) and the Key Scientific and Technological Team from innovation Shaanxi Province (No.2015KCT-12).

References

1. H. Chen, X. Wang, J. Li and X. Wang, *J. Mater. Chem. A*, 2015, **3**, 6073-6081.
2. F. Mou, D. Pan, C. Chen, Y. Gao, L. Xu and J. Guan, *Adv. Funct. Mater.*, 2015, **25**, 6173-6181.
3. H.-Y. Jing, T. Wen, C.-M. Fan, G.-Q. Gao, S.-L. Zhong and A.-W. Xu, *J. Mater. Chem. A*, 2014, **2**, 14563-14570.

4. K.-T. Lee and S.-Y. Lu, *J. Mater. Chem. A*, 2015, **3**, 12259-12267.

5. L. Wang, C. Cheng, S. Tapas, J. Lei, M. Matsuoka, J. Zhang and F. Zhang, *J. Mater. Chem. A*, 2015, **3**, 13357-13364.

6. X. Zhang, J. Liu, S. Kelly, X. Huang and J. Liu, *J. Mater. Chem. A*, 2014, **2**, 11759-11767.

7. S. Xing, D. Zhao, W. Yang, Z. Ma, Y. Wu, Y. Gao, W. Chen and J. Han, *J. Mater. Chem. A*, 2013, **1**, 1694-1700.

8. M. A. Shannon, P. W. Bohn, E. Menachem, J. G. Georgiadis, B. J. Marias and A. M. Mayes, *Nature*, 2008, **452**, 301-310.

9. J. S. Hu, L. S. Zhong, W. G. Song and L. J. Wan, *Adv. Mater.*, 2008, **20**, 2977-2982.

10. B. Youn-Sang and R. Q. Snurr, *Angew. Chem. Int. Ed.*, 2011, **50**, 11586-11596.

11. B. Wang, H. Wu, L. Yu, R. Xu, T. T. Lim and X. W. Lou, *Adv. Mater.*, 2012, **24**, 1111-1116.

12. J. B. Fei, Y. Cui, X. H. Yan, W. Qi, Y. Yang, K. W. Wang, Q. He and J. B. Li, *Adv. Mater.*, 2008, **20**, 452-456.

13. L. Ai, Y. Zhou and J. Jiang, *Desalination*, 2011, **266**, 72–77.

14. L. Ai, H. Huang, Z. Chen, X. Wei and J. Jiang, *Chem. Eng. J.*, 2010, **156**, 243–249.

15. M. Rafatullah, O. Sulaiman, R. Hashim and A. Ahmad, *J. Hazard. Mater.*, 2010, **177**, 70-80.

16. L. Ai, J. Jiang and R. Zhang, *Synthetic Met.*, 2010, **160**, 762-767.

17. A. K. Bhattacharya, T. K. Naiya, S. N. Mandal and S. K. Das, *Chem. Eng. J.*, 2008, **137**, 529–541.

18. D. Mohan and C. U. Pittman, *J. Hazard. Mater.*, 2007, **142**, 1–53.

19. S. Wang, H. Li and L. Xu, *J. Colloid Interf. Sci.*, 2006, **295**, 71–78.

20. F. Delval, G. Crini and J. Vebrel, *Bioresource Technol.*, 2006, **97**, 2173-2181.

21. L. S. Zhong, J. S. Hu, A. M. Cao, Q. Liu, W. G. Song and L. J. Wan, *Chem. Mater.*, 2007, **19**, 1648-1655.

22. R. Chen, J. Yu and W. Xiao, *J. Mater. Chem. A*, 2013, **1**, 11682-11690.

23. W. Liu, X. Zhao, T. Wang, J. Fu and J. Ni, *J. Mater. Chem. A*, 2015, **3**, 17676-17684.

24. X. Li, Z. Si, Y. Lei, X. Li, J. Tang, S. Song and H. Zhang, *Crystengcomm*, 2010, **13**, 642-648.

25. Y. X. Zhang, X. Y. Yu, Z. Jin, Y. Jia, W. H. Xu, T. Luo, B. J. Zhu, J. H. Liu and X. J. Huang, *J. Mater. Chem.*, 2011, **21**, 16550-16557.

26. Y. X. Zhang, Y. Jia, Z. Jin, X. Y. Yu, W. H. Xu, T. Luo, B. J. Zhu, J. H. Liu and X. J. Huang, *Crystengcomm*, 2012, **14**, 3005-3007.

27. Y. Xia, X. Jiao, Y. Liu, D. Chen, L. Zhang and Z. Qin, *J. Phys. Chem. C*, 2013, **117**, 15279-15286.

28. W. Cai, J. Yu, B. Cheng, B. L. Su and M. Jaroniec, *J. Phys. Chem. C*, 2009, **113**, 14739-14746.

29. E. Kumar, A. Bhatnagar, W. Hogland, M. Marques and M. Sillanpää, *Chem. Eng. J.*, 2014, **241**, 443-456.

30. S. Liu, C. Chen, Q. Liu, Y. Zhuo, D. Yuan, Z. Dai and J. Bao, *RSC Adv.*, 2015, **5**, 71728-71734.

31. X. Y. Chen, Z. J. Zhang, X. L. Li and S. W. Lee, *Solid State Commun.*, 2008, **145**, 368–373.

32. A. J. McCue, A. M. Shepherd and J. A. Anderson, *Catal. Sci. Technol.*, 2015, **5**, 2880-2890.

33. W. Cai, J. Yu and M. Jaroniec, *J. Mater. Chem.*, 2010, **20**, 4587-4594.

34. T. Kim, J. Lian, J. Ma, X. Duan and W. Zheng, *Cryst. Growth Des.*, 2010, **10**, 2928-2933.

35. E. Yu, H. J. Lee, T. J. Ko, S. J. Kim, K. R. Lee, K. H. Oh and M. W. Moon, *Nanoscale*, 2013, **5**, 10014-10021.

36. H. Liang, L. Liu, H. Yang, J. Wei, Z. Yang and Y. Yang, *Crystengcomm*, 2011, **13**, 2445-2450.

37. D. Kang, S. Tong, X. Yu and M. Ge, *RSC Adv.*, 2015, **5**, 19159-19165.

38. H. Huang, L. Wang, Y. Cai, C. Zhou, Y. Yuan, X. Zhang, H. Wan and G. Guan, *Crystengcomm*, 2015, **17**, 1318-1325.

39. X. Song, P. Yang, C. Jia, L. Chen and K. Matras-Postolek, *RSC Adv.*, 2015, **5**, 33155-33162.

40. S. Lan, N. Guo, L. Liu, X. Wu, L. Li and S. Gan, *Appl. Surf. Sci.* 2013, **283**, 1032-1040.

41. W. Cai, J. Yu, S. Gu and M. Jaroniec, *Cryst. Growth Des.*, 2010, **10**, 3977-3982.

42. X. Wang, C. Zhan, B. Kong, X. Zhu, J. Liu, W. Xu, W. Cai and H. Wang, *J. Colloid Interf. Sci.*, 2015, **453**, 244-251.

43. J. Ge, K. Deng, W. Cai, J. Yu, X. Liu and J. Zhou, *J. Colloid Interf. Sci.*, 2013, **401**, 34-39.

44. Y. Feng, W. Lu, L. Zhang, X. Bao, B. Yue, Y. Lv and X. Shang, *Cryst. Growth Des.*, 2008, **8**, 1426-1429.

45. W. Cai, J. Yu and S. Mann, *Micropor. Mesopor. Mater.*, 2009, **122**, 42–47.

46. Q. Feng, Z. Zhang, Y. Ma, X. He, Y. Zhao and Z. Chai, *Nanoscale Res. Lett.*, 2012, **7**, 84.

47. S. H. Xuan, F. Wang, X. L. Gong, S. K. Kong,. J. C. Yu and. K. C.-F. Leung, *Chem. Commun.*, 2011, **47**, 2514-2516.

48. C. L. Fang, K. Qian, J. Zhu, S. Wang, X. Lv and S. H. Yu, *Nanotechnology*, 2008, **19**, 125601.

49. S. H. Xuan, Y. X. J. Wang, J. C. Yu and K. C-F. Leung, *Langmuir*, 2009, **25**, 11835-11843.

50. L. S. Zhong, J. S. Hu, H. P. Liang, A. M. Cao, W. G. Song and L. J. Wan, *Adv. Mater.*, 2006, **18**, 2426–2431.

51. X. Y. Yu, T. Luo, Y. Jia, R. X. Xu, C. Gao, Y. X. Zhang, J. H. Liu and X. J. Huang, *Nanoscale*, 2012, **4**, 3466-3474.

52. Y. Li, F. Liu, X. Bing, Q. Du, Z. Pan, D. Wang, Z. Wang and Y. Xia, *J. Hazard. Mater.*, 2010, **177**, 876-880.

53. Y. X. Zhang, Z. L. Liu, B. Sun, W. H. Xu and J. H. Liu, *Rsc Adv.*, 2013, **3**, 23197-23206.

54. C. Y. Cao, J. Qu, W. S. Yan, J. F. Zhu, Z. Y. Wu and W. G. Song, *Langmuir*, 2012, **28**, 4573-4579.

55. Y. Wang, G. Wang, H. Wang, W. Cai, C. Liang and L. Zhang, *Nanotechnology*, 2009, **20**, 155604.

56. Y. X. Zhang and Y. Jia, *Appl. Surf. Sci.*, 2014, **290**, 102-106.

57. Y. Jia, X. Y. Yu, T. Luo, M. Y. Zhang, J. H. Liu and X. J. Huang, *Dalton T.*, 2013, **42**, 1921-1928.

58. S. Mor, K. Ravindra and N. R. Bishnoi, *Bioresource Technol.*, 2007, **98**, 954–957.

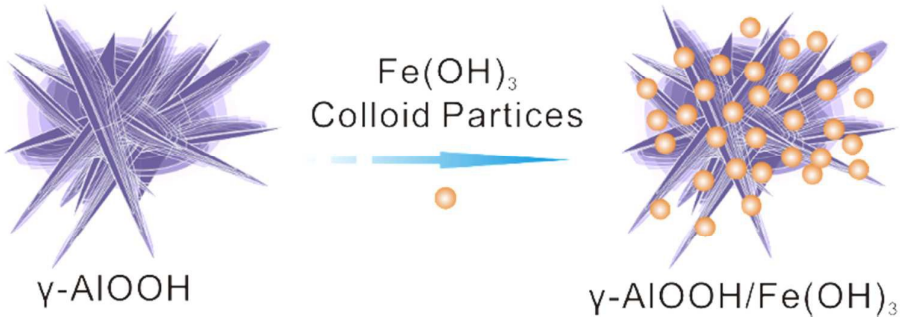

Monodispersed γ-AlOOH/$Fe(OH)_3$ with hierarchical structures have been prepared, which show an excellent performance for As(V) and Cr(VI) removal.